

Structural vibration quantification of micro wind turbine-building system using a novel finite element analysis

Bo Ren

College of Mobile Telecommunications, Chongqing University of Posts and Telecom, Hechuan, Chongqing 401520, People's Republic of China
E-mail: gongchengshi123@163.com

Published in *The Journal of Engineering*; Received on 9th March 2016; Accepted on 25th May 2016

Abstract: For turbine generated building vibration used in wind power industry, estimation of excitation/contact force at the connecting point between turbine and building structure is one of main concerns for Lab simulation of turbine. However, the Lab simulation method aiming at achieving both accurate simulation of working environment of turbine and the corresponding vibration level prediction/quantification of building response is not available so far. The direct force measurement method was investigated and found to be practically impossible in terms of operational accessibility. A method for indirectly determining interface contact force is proposed for Lab simulated, motor replaced, free stand wall mounted building vibration prediction. Power supply for driving the turbine and rotational speed automatic control of turbine for Lab simulation were determined by the proposed method. Furthermore, the establishments of suitable finite element models with their validation achieved good prediction results within acceptable error scales.

1 Introduction

A vast number of small wind turbine mounted building used in wind energy industry and renewable technology are developed in the past few years in UK as a novel technique for the usage of wind power. The utilisation of building-mounted micro wind turbine can be more effective, applicable, flexible and low cost than the traditional large wind mill/farm. However, before mounting this particular small turbine, it is necessary to predict the vibration levels of building which generated from the turbine during its working period. This prediction will help the engineer to make a decision whether this site is suitable for mounting a small wind turbine or not.

In the past few decades, finite element models (FEMs) had been demonstrated as a good tool to predict vibration accurately. The basic theory of FE analysis (FEA) for vibration prediction could be found in Stephen Timoshenko's series of books regarding structural mechanics. The previous research and effort toward vibration prediction using FEMs has been reviewed below to find out what we need to know to perform an effective FEA for the purpose of vibration prediction. Above all, Wilson and Habibullah [1] had stated for the purpose of this prediction, the FE computer program such as ANSYS were used in this paper. In this program, the user should define the type of FE which constitutes the structure. To model the free stand wall of the building which the turbine mounted on in the Lab (Fig. 1), shell elements were used since this type of free stand wall would be considered as a plate structure in the theory of [2] according to the shape and geometry of it (the ratio of thickness/width <0.1). Shell elements in ANSYS are four-node elements with six degrees of freedom (DOFs) at each node, and were used for the three-dimensional-FEMs. Moreover, each element can be assigned a set of material properties such as masonry or brickwork in this paper.

The material properties include E (Young's modulus), ν (Poisson's ratio) and ρ (density) of the masonry in this paper. Some literatures should be reviewed before estimating the correct values of these parameters. Poisson's ratio had been demonstrated to have a minimal effect on the structural dynamic response of the structure in the previous research and thus a constant value of 0.25 is assigned, as recommended by most of the researchers [3–6].

Regarding the Young's modulus, Europe Standard EN 1996-1-1 (2005) [7] had been reviewed. The following tabulated values are

recommended by EN 1996-3: 2006 [8]; they are derived from EN 1996-1-1:2005 (Table 1).

Note:

- The modulus of elasticity should be determined by both the motor types and compressive strength f_b .
- Light weight mortar: mortar with a dry hardened density equal to 1300 kg/m³ according to EN 998-2 [9].
- Clay units Groups 1, 2, 3 and 4: group classifications for clay units, according to the volume (%) and orientation of all holes (Table 2).

Clay facing masonry units maybe classified in accordance with the gross dry density classes given in Table 3 [10].

Sassoni *et al.* [5] compared Young's modulus of bricks and mortar for two masonry types. For first type, $E_b = 10.0$ GPa, $E_m = 9.0$ GPa; for second one, $E_b = 6.5$ GPa, $E_m = 6.3$ GPa. Table 4 presents the numerical scale of Young's modulus and density derived from Erdogmus and Boothby [6]'s work. The upper and lower limits were determined by both Erdogmus and Boothby [6]'s tests and the extensive manual of [11].

Furthermore, Nichols and Totoev [3] undertook a more extensive and broad investigation on all the material properties for up to five types of bricks as shown in the next table (Table 5).

As a guidance of reviewing the above standards and literatures, the final values of material properties could be determined and measured by a series of static testing in Lab and the results were obtained as follows (Table 6).

After the preliminary work above completed, the initial FE model was built up in ANSYS. Moreover, the boundary conditions (BCs) should be determined in ANSYS. Since the free stand wall is resting on the concrete floor without moving, the contact surface between them at the bottom of wall should be considered as fixed.

Here is a more complex BC at the left edge of the wall which requires paying more attention to. The real connection (Fig. 2) between the free stand wall and another concrete column/outside wall of the building is only made of mortar or clay, as shown in the geometric model (Fig. 3). It could be considered as a clay strip (Fig. 4a) according to its geometry of connection (Fig. 4b) when we did a further detailed investigation. This is a similar pinned connection (Fig. 4c) in Timoshenko's article [2] regarding

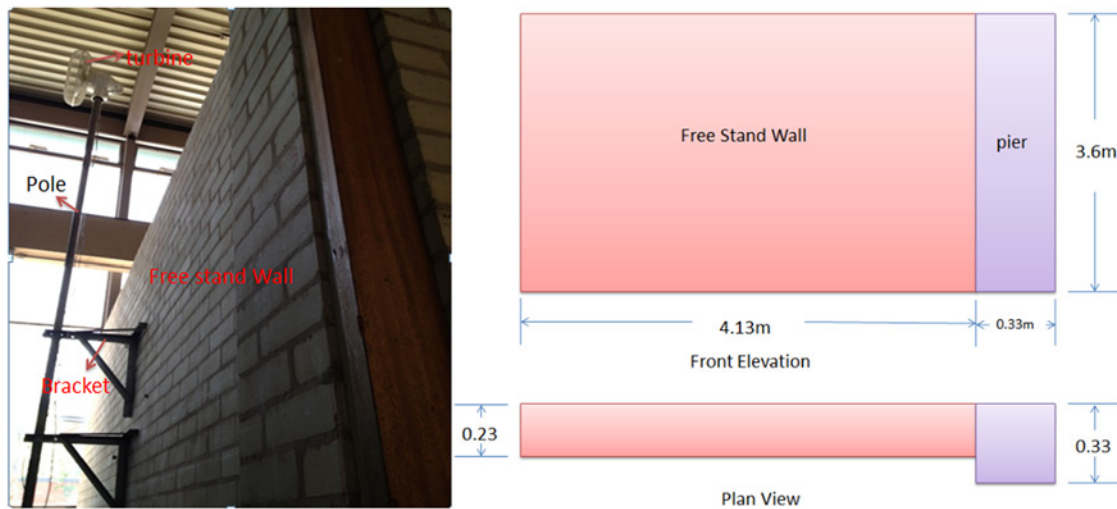


Fig. 1 Free stand wall of building which needs to be modelled in FE program

the analysis of BC/constraints for plate and shell. It is described as following for pinned edge: if the edge of the plate (Fig. 4c) is pinned supported, the deflection of this edge should be zero: $(w)_{x=a} = 0$. At the same time, this edge can rotate with no restrictions and bending moments M_x along this edge: $((\partial^2 w / \partial x^2) + \nu (\partial^2 w / \partial y^2))_{x=a} = 0$. In ANSYS, we would define the edge: $(w)_{x=a} = 0$; $(\partial w / \partial x) \neq 0$; $(\partial w / \partial y) = 0$ (Fig. 5).

2 Theoretical modal analysis

If we perform one type of structural analysis of FEA which is called theoretical modal analysis, the physical model of free stand wall will be replaced by a geometrical model of a thin plate structure in ANSYS, assume that x and y are the axes which parallel to the plane of the plate. According to the classic plate theory from [2], only pure bending was taken into account (an assumption was made to ignore the shear force and torsion). This will reflect the application of DOFs: only three DOFs considered: translational movement of z -axis (UZ), rotational movement of x (ROTX) and y axes (ROTY).

The results of theoretical modal analysis include some important structural parameters of vibration: such as natural/modal frequency and the corresponding mode shape at each mode (Table 7 and Fig. 6).

These parameters will be used to predict/determine the vibration levels in another type of structural analysis, for example, harmonic analysis in this paper. Before post-processing to another analysis, these parameters should be validated by experimental results for robust or rigorous purpose.

3 Experimental modal analysis/structural testing/impact testing

Before validation, we should do the experimental modal analysis to obtain the experimental modal parameters. This could be achieved by finishing an impact testing of structural testing which had been widely applied in automotive engineering.

In this paper, the author employed the measurement equipment from a professional company focused on vibration and structural dynamics which is called LMS LTD in Belgium. The required measurement data for impact testing are the impact forces which were excited by an impact hammer and the corresponding vibration response of the wall generated by the impact. The force would be measured by the force transducer mounted on the head of the hammer and the response measured by the accelerometer. Both of them are IEPE transducers (DEVECO impulse hammer, sensitivity: 1 mv/1 bf; PCB 336c accelerometer, sensitivity: 1000 mv/g). IEPE refers to an ICP transducer with a built-in charge or voltage

amplifier to amplify and condition the signal since signal is very small and susceptible to noise.

Both of the two sets of signal data were received by a data acquisition (DAQ) equipment (such as LMS Pimento in this paper). The professional software (such as LMS test xpress 7A & LMS Lab Test 12B) was used to analyse these data to obtain the corresponding modal parameters of the wall (Fig. 7).

However, several points on the wall need to be measured if we want to obtain the results as this is required by the impact testing. Hence, the surface of the wall has to be grid into different response points (RPs), as shown in Fig. 8.

Once the whole testing was completed, the corresponding experimental modal parameters would be calculated by the post-processing of software. Moreover, these results (Table 8 and Fig. 9) would be referred in a further validation process.

4 Natural frequencies' updating

If we compare the initial theoretical and experimental natural frequency (Table 9), all the errors in percentage were significant for each mode. To investigate the degree of correlation of the two sets of parameters, a plot of them against by each other in each mode separately was shown in Fig. 10. From this figure, it is straightforward to find that the correlation is so low ($k = 0.64$) that the deviation from best fit ($k = 1$) is large ($\delta = 35.97\%$). To eliminate the difference and toward the target, an updating process should be considered. There are several aspects under investigation for the purpose of validation.

4.1 Material properties (first updating)

It has been said that FEA overestimates stiffness [12–14]. This error will result in an overestimation of the natural frequency, since $f = \sqrt{k/m}$. However, the material properties' input for FEA are Young's modulus and density, their relationship to frequency is $f \propto \sqrt{E/\rho}$. Hence, a slight decrease of E or increase of ρ would reduce the overestimation. Both variations were performed within the appropriate boundaries scale ($E: 10.5 \rightarrow 10$ GPa; $\rho: 2130 \rightarrow 2270$ kg/m³). Table 10 and Fig. 11 show the comparison results after first updating.

The results indicate a slight improvement of correlation and a reduction both in error and deviation. The slope has also been improved from 0.640 to 0.677; an upgrading of 0.037 toward the target (best correlation), only 0.323 (32.3%) away from unity.

4.2 Pier-like sub-structure (second update)

As a raw estimation, the initial FE model considered the free stand wall as a fully rectangular plate (Fig. 12) with a regular thickness

Table 1 Elasticity of modulus of masonry

Masonry units group 1									
$f_b, \text{N/mm}^2$	General purpose mortar				Thin joint	Light weight mortar			
	M2.5	M5	M10	M20		M2.5	M5	M10	
2	1200	1400	1400	1400	1400	600	700	700	
4	1900	2400	2700	2700	2400	1000	1300	1500	
6	2500	3100	3800	4100	3400	1400	1700	2100	
8	3100	3800	4700	5400	4400	1700	2100	2600	
10	3600	4500	5500	6800	5300	2000	2400	3000	
12	4100	5100	6200	7700	6200	2200	2800	3400	
16	5000	6200	7600	9400	7900	2800	3400	4200	
20	5900	7300	8900	11,000	9600	3200	4000	4900	
25	6900	8500	10,400	12,900	11,600	3800	4600	5700	
30	7800	9600	11,900	14,600	13,500	4300	5300	6500	
50	11,200	13,800	17,000	20,900	20,900	6100	7500	9300	
75	14,900	18,300	22,500	27,700	20,900	8100	10,000	12,300	
Masonry units group 2									
$f_b, \text{N/mm}^2$	General purpose mortar				Thin joint	Light weight mortar			
	M2.5	M5	M10	M20		M2.5	M5	M10	
2	1000	1100	1100	1100	1100	500	600	600	
4	1600	1900	2200	2200	1800	900	1100	1200	
6	2100	2600	3100	3300	2500	1200	1400	1700	
8	2500	3100	3800	4400	3000	1400	1700	2100	
10	3000	3700	4500	5500	3500	1600	2000	2500	
12	3400	4200	5100	6300	4000	1900	2300	2800	
16	4100	5100	6300	7700	4900	2300	2800	3500	
20	4800	5900	7300	9000	5700	2700	3300	4100	
25	5600	6900	8500	10,500	6700	3100	3900	4700	
30	6400	7900	9700	12,000	7600	3600	4400	5400	
50	9200	11,300	13,900	17,100	10,800	5100	6300	7700	
75	12,200	15,000	18,400	22,700	10,800	6800	8300	10,200	
Masonry units groups 3 and 4									
$f_b, \text{N/mm}^2$	General purpose mortar				Thin joint		Light weight mortar		
	M2.5	M5	M10	M20	Group 3	Group 4	M2.5	M5	M10
2	700	900	900	900	0800	600	400	500	500
4	1200	1500	1700	1700	1300	1100	700	900	1000
6	1600	2000	2400	2600	1800	1600	900	1100	1400
8	2000	2400	3000	3400	2100	2000	1100	1400	1700
10	2300	4500	3500	4300	2500	2500	1300	1600	2000
12	2600	5100	4000	4900	2800	2900	1500	1800	2300
16	3200	6200	4900	6000	3500	3700	1800	2300	2800
20	3800	7300	5700	7000	4100	4500	2100	2600	3200
25	4400	5400	6600	8200	4800	5400	2500	3100	3800
30	5000	6100	7600	9300	5400	6300	2800	3500	4300
50	7100	8800	10,800	13,300	7700	9700	4100	5000	6200
75	9500	11,600	14,300	17,700	7700	9700	5400	6700	8200

Table 2 Conditions for grouping of clay units

Materials and thresholds for clay units					
	Group 1 (all materials)		Group 2	Group 3	Group 4
	Units		Vertical holes		Horizontal holes
Volume of all holes, %	≤25	clay	>25; ≤55	≥25; ≤70	>25; ≤70

(0.22 m). However, this is not the real case actually. There is a pier-like sub-structure (masonry column) at the right column which has a different thickness (0.33 m) and it acts like a stiffening member (Fig. 13). This member would be considered alone as an independent sub-structure with defined thickness when modelling in ANSYS. Then, the second update results were presented in Table 11 and Fig. 14.

It looks more complex regarding this update, the error in some modes became larger and the others otherwise. Thus, it is difficult to judge whether there is an improvement or not. Hence, it is necessary to check the correlation slope. As seen from the correlation

Table 3 Classification of clay masonry units based on gross dry density

Gross dry density class	Density range, kg/m ³
2.4	>2200
2.2	2010–2200
2.0	1810–2000
1.8	1610–1800
1.6	1410–1600
1.4	1210–1400
1.2	1010–1200
1.0	905–1000
0.9	805–900
0.8	705–800
0.7	605–700
0.6	505–600
0.5	≤500

Table 4 Scale of Young's modulus and density of brickworks as required

Component	Material type	Modulus of elasticity		Density
walls	brick	low, GPa	high, GPa	nominal, kg/m ³
		7.5	11	2100

figure, the deviation of the third mode improved a lot and the trend line looked like much smoother now. However, this did not affect the overall improvement of slope much, a total poor improvement (only 0.0021 from 0.6773 to 0.6794) of correlation slope toward the target and sight updating (<1%). This indicated that pier sub-structure does not play an important role for the change of modal parameters and structural behaviour.

4.3 Elastically supported built-in end (third update)

In the initial model, two BCs were applied: fixed end at the bottom and pinned end at the left edge. However, neither fixed nor pinned constrain occurs in real structural connections. In few cases, a fixed or pinned BC approximation maybe a close enough representation of reality; otherwise, the BC should be approximated realistically by a semi-fix (or semi-flexible) representation.

Timoshenko and Woinowsky-Krieger [2]'s book considered this particular case of BC (Figs. 1–4), they simplified the case to an elastically supported or elastically built-in edge which described as follows: they assumed a rectangular plate is elastically coupled to a supporting beam-like structure (Fig. 15), the displacement of this interface is equal to the deflection of the beam. This will employ the beam elements (BEAM188) with one fixed end to represent the elastic property of BC in ANSYS. This element is a linear two-node beam element in 2D FEM. However, the MATRIX27 element for more complex linear beams seems to be a better option due to its unique aptitude to allow the user full control of input parameters. Its structural dynamic response can be described

Table 5 Material properties of five brick types

Brick type	Young's modulus, MPa	Poisson's ratio	Density, kg/m ³
pressed clay red	14,000	0.22	2320
pressed clay	10,000	0.29	2270
biscuit			
pressed clay brown	7000	0.21	2130
calcium silicate	6000	0.17	1760
concrete	14,000	0.33	2190

Table 6 Physical properties used in the initial FE model

Parameter	Value
Young's modulus E , N/m ²	10.5×10^9
Density ρ , kg/m ³	2130
Poisson's ratio	0.25

by stiffness in matrix form. The matrices of this element are 12×12 . If one node is fixed without movement, let all rows and columns of this node default to zero. The stiffness matrix constants are input as real constants. These constants could be calculated from the well-known established slope/deflection equations for a beam of flexural rigidity EI , the element stiffness matrix of Euler–Bernoulli Beam with length l_e can be shown as follows.

Fig. 15 elastic connection performed in FE model of ANSYS

$$k_e = EI \begin{bmatrix} \frac{12}{l_e^3} & \frac{6}{l_e^2} & -\frac{12}{l_e^3} & \frac{6}{l_e^2} \\ & \frac{4}{l_e} & -\frac{6}{l_e^2} & \frac{2}{l_e} \\ & & \frac{12}{l_e^3} & -\frac{6}{l_e^2} \\ \text{sym.} & & & \frac{4}{l_e} \end{bmatrix} \quad (1)$$

The young's modulus E in the equation is uncertain and expected to be estimated from a relative high value (e.g. value of concrete) to a gradually decreased value toward the target. From the previous Lab tests by [15], the measured modulus of elasticity of concrete was 30.00 GPa. The values of I and l_e were obtained from the geometry of length and cross-section of the supporting beam (clay strip in Fig. 4), the support stiffness were finally calculated from the above information (take $E = 14$ GPa as an example)

$$k_e = \begin{bmatrix} 6.02 & 4.2 & -6.02 & 4.2 \\ 4.2 & 3.99 & -4.2 & 2 \\ -6.02 & -4.2 & 6.02 & -4.2 \\ 4.2 & 2 & -4.2 & 3.99 \end{bmatrix} \times 10^5 \quad (2)$$

Equation 3 indicates the stiffness matrix developed particularly for ANSYS

$$k_e = \begin{bmatrix} 0 & 0 & 0 & 0 & 0 & 0 & 0 & 0 & 0 & 0 & 0 & 0 \\ 0 & 0 & 0 & 0 & 0 & 0 & 0 & 0 & 0 & 0 & 0 & 0 \\ & 6.02 & 4.2 & 0 & 0 & 0 & 0 & -6.02 & 4.2 & 0 & 0 & 0 \\ & & 3.99 & 0 & 0 & 0 & 0 & -4.2 & 2 & 0 & 0 & 0 \\ & & & 0 & 0 & 0 & 0 & 0 & 0 & 0 & 0 & 0 \\ & & & & 0 & 0 & 0 & 0 & 0 & 0 & 0 & 0 \\ & & & & & 0 & 0 & 0 & 0 & 0 & 0 & 0 \\ & & & & & & 0 & 0 & 0 & 0 & 0 & 0 \\ & & & & & & & 6.02 & -4.2 & 0 & 0 & 0 \\ & & & & & & & & 3.99 & 0 & 0 & 0 \\ & & & & & & & & & 0 & 0 & 0 \\ & & & & & & & & & & 0 & 0 \\ & & & & & & & & & & & 0 \end{bmatrix} \times 10^5 \quad (3)$$

The results of natural frequencies predicted by ANSYS are located in Table 12 and Fig. 16 when compared with the measured data ($E = 14$ GPa).

If gradually increasing the Young's modulus (E) from zero (free edge) to more than 40 GPa (toward rigid/fixed edge), the correlation



Fig. 2 Picture of the connection

improved very slow if E beyond the saturation point where $E = 14$ GPa (Fig. 17) and the best correlation could be confirmed as 0.6942.

It is concluded that a more accurate BC affects the correlation significantly. The slope of the trend line has changed from 0.6794 to 0.6942, a better fit toward target of 0.0148 and 0.3058 (30.58%) away from perfect correlation.

4.4 Fine tuning

Fine tuning was based on the first updating regarding material properties of masonry and was carefully tuned to make small adjustments to perfect correlation. Hence, the Young's modulus of masonry was decreased slightly to 9.75 GPa and its density was increased to 2320 kg/m³. It is accepted that the former is inside the range of values given in the previous test and also the European Standard. The density still lies in the scale of the bounds given by British Standard. The results from the tuning are showed in Table 13 and Fig. 18.

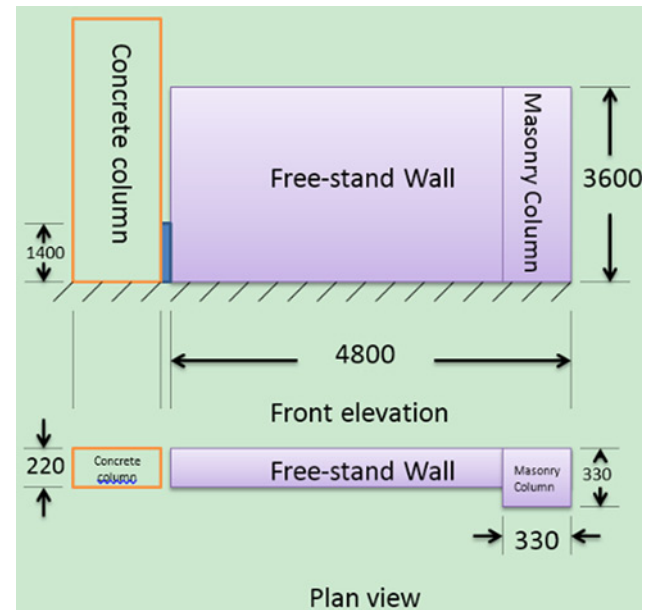
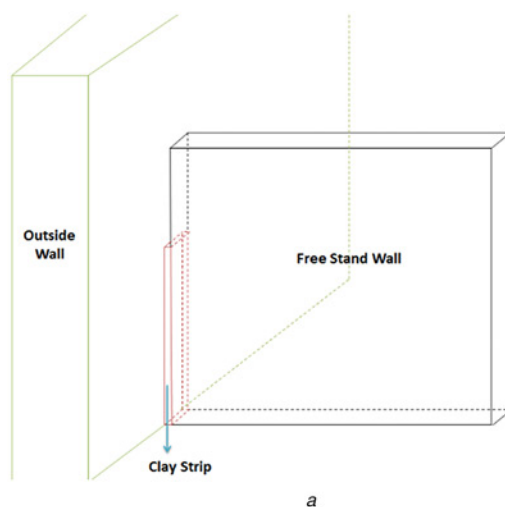


Fig. 3 Connection in the geometric model

Fine tuning updated the trend line slope of a former value 0.6942 to improved value 0.7114. This is an improvement toward target of only 0.0172 but it can easily be verified and justified in the FEM updating process. The final validated value is 0.2886 (28.86%) away from perfect correlation and could be updated further in the next FEA.

5 Commentary on the results

The major arguments in terms of the results have been discussed in the previous Section 4 but two supplementary comments still need to be clarified. It should be stressed that correlation relationship depends on many variables but their degree of sensitivity varies. Correlation is special sensitive to the material properties of brick-work and the boundary edges of the masonry structure. Fig. 19a indicates how far the actual correlation is deviated from the target value of best fit for each updating procedure. The results of 3.7% between the preliminary model and the one after first update and

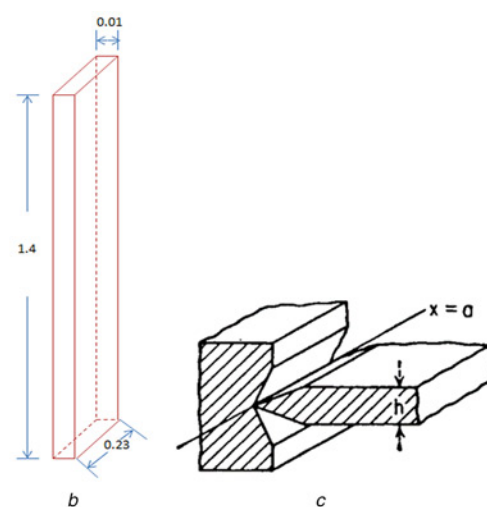


Fig. 4 Clay strip
a Clay strip connection
b Clay strip's geometry
c Timoshenko pin restraint

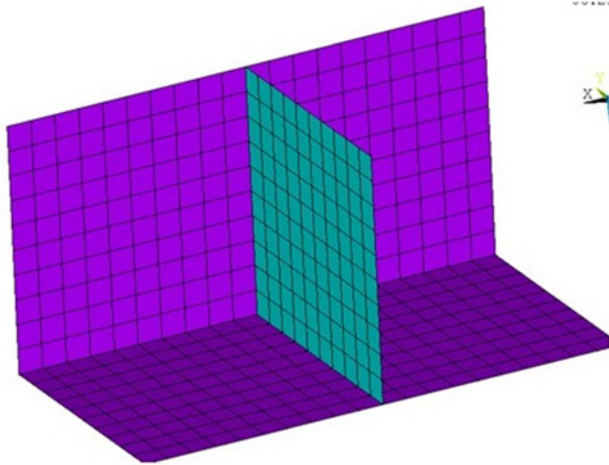


Fig. 5 FEM with pin connection in ANSYS

Table 7 Initial predicted natural frequencies

Mode number	Predicted frequency, Hz
1	6.4953
2	14.395
3	37.820
4	41.869
5	53.054

that of 1.48% between the second and third updates explain why the material properties and BCs are the most important variables which need careful consideration during the updating process. Similarly, Fig. 19b shows relative improvements in an effort toward best fit of unity.

6 Mode shapes' updating

The mode shapes' updating process could be repeated by the procedures stated above in a similar way. The only term needed to be mentioned here is the tool for comparing predicted and measured mode shapes, which is called the modal assurance criterion (MAC). The MAC value between two different normal modes $\{\psi\}_r$ and $\{\psi\}_s$ which is defined as

$$MAC_{rs} = \frac{|\{\psi\}_r^H \{\psi\}_s|^2}{(\{\psi\}_r^H \{\psi\}_r)(\{\psi\}_s^H \{\psi\}_s)} \quad (4)$$

which can be interpreted as the correlation coefficient between the two mode shape matrices. MAC is a value between 0 and 1 which detects the similarity of the two modes. Fig. 20 shows MAC value

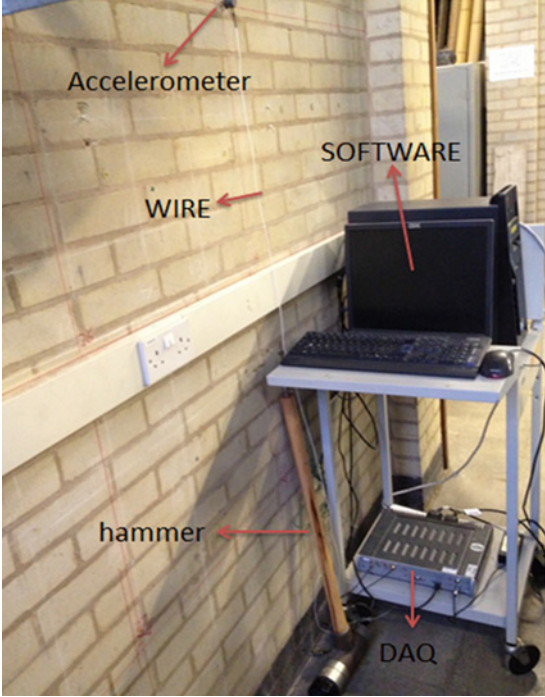


Fig. 7 Measurement equipment for impact testing

between the initial FE model and experimental mode shapes. As seen from figure, the similarity of several modes of the original ANSYS FE models compared with experimental results were displayed and for which mode shapes do not change excessively (with $MAC > 0.9$) are shown as dark purple in MAC column of Fig. 20. The remainder of the experimentally identified modes and the other modes predicted by FEM whose correspondence is less clear (with $MAC < 0.9$) are nonetheless important characteristics of the system (light colour).

With a statistically updating process similarly to natural frequency stated in the last section, the correlation between two different sets of mode shapes had been improved and shown as an overhead view in Fig. 24. This had been drawn from the comparison results between the original FE model and the 'improved' FEM which benefited from the updating changes described in the previous section. Of most interest is the observation that several modes in the improved models do not correspond with any from the original model. This is a surprising observation given that only relatively minor modification was made to change the FEM. It should be noted that when referring the figure generally the graphs MAC calculations give the highest number of correlated mode pairs with least ambiguity (the optimal mode number 15 chosen for this case) (Fig. 21).

It is clear to see from the MAC calculation graphs that the number of closely correlated modes ($MAC > 0.9$) became obviously more and the updating process particularly improved the relationship for the first

Mode No.	1	2	3	4	5
Mode shape					

Fig. 6 Theoretical mode shapes

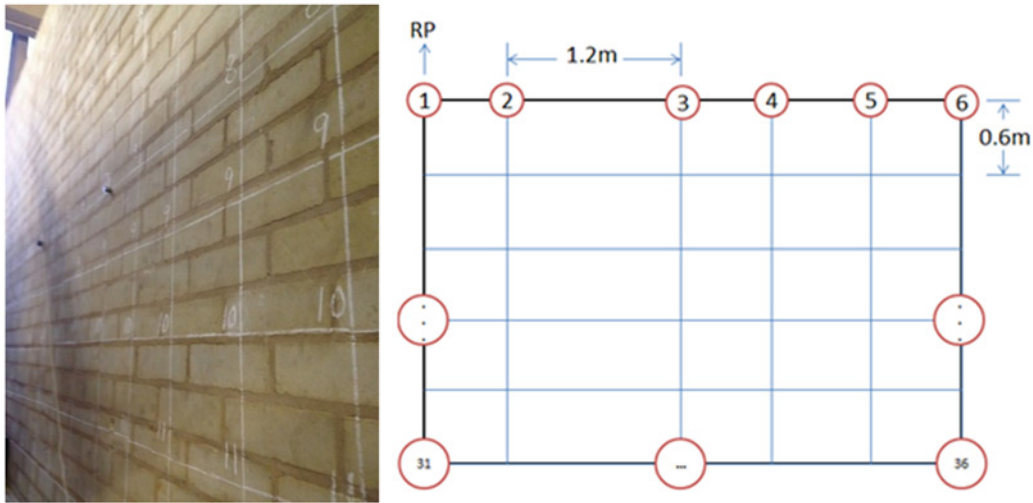


Fig. 8 Different vibration RPs under measurement

Table 8 Measured natural frequency

Mode number	Measured frequency, Hz
1	3.678
2	9.589
3	21.067
4	27.860
5	34.194

few modes up to 7. Furthermore, none of the modes of $MAC < 0.8$ existed after updating. This demonstrated that all the modes perform a good and acceptable correlation between prediction and measurement after a series of updating process.

7 Harmonic analysis

After validating both of the natural frequencies and mode shapes, the modal parameters look robust now for further prediction of vibration response. Harmonic analysis in FEA is an effective method to predict the structural behaviour using the results from theoretical modal analysis in conjunction with known force input. A harmonic analysis is used to determine the response of the structure under a steady-state sinusoidal (harmonic) loading at a given frequency. This is in accordance with the working principle of wind turbine with a rotational speed [revolutions per minute (RPM)]/frequency. In a harmonic analysis, the loading/force and response/vibration level of the structure is assumed to be harmonic (cyclic)

$$f(t) = F(\omega) \sin \omega t$$

$$x(t) = X(\omega) \sin \omega t, \quad \text{where } \omega = 2\pi f; f = \frac{\text{RPM}}{60} \quad (5)$$

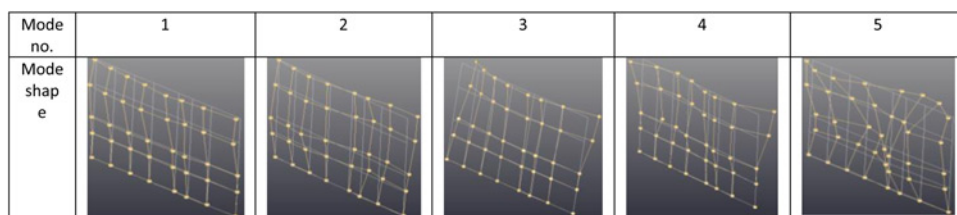


Fig. 9 Measured mode shape

Table 9 Comparison of initial predicted and measured frequencies

Mode number	Measured frequency, Hz	Predicted frequency, Hz	Error, %
1	3.678	6.4953	43.37444
2	9.589	14.395	33.38659
3	21.067	37.820	44.29667
4	27.860	41.869	33.45912
5	34.194	53.054	35.54869

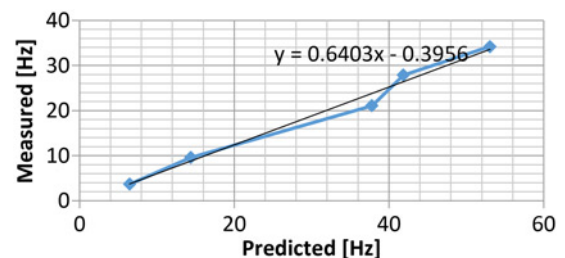


Fig. 10 Initial prediction against measurement

7.1 Force identification (a new indirect/inverse force estimation method)

According to the explanation from above paragraph, in order to perform a harmonic analysis, the excitation contact force/loading between turbine and wall should be estimated or measured. The straightforward way to quantify the contact force is a direct force measurement method using a force transducer between turbine and wall. However, this was difficult in practical: assuming a contact interface

Table 10 New error after first update

Mode number	Measured, Hz	Predicted, Hz	Error, %
1	3.678	6.1401	40.0987
2	9.589	13.608	29.5341
3	21.067	35.752	41.0746
4	27.86	39.580	29.6109
5	34.194	50.153	31.8206

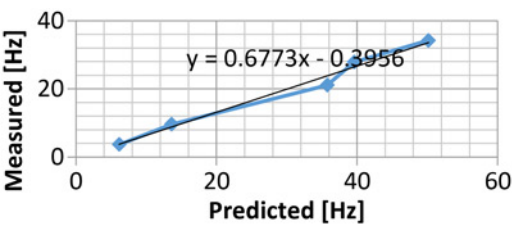


Fig. 11 Improved correlation after first update

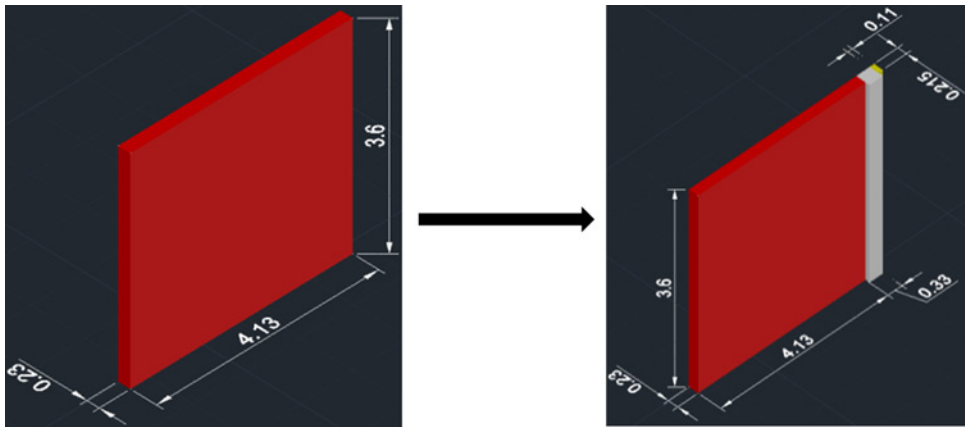


Fig. 12 Initial assumption to second update

constitute of a set of single points, the direct measurement of forces exerted on the interface maybe possibly achieved by inserting a force transducer with good calibration results between the turbine and wall/building at the interface points. For simplified situation where a source is contacted/connected with a receiver at one single point in 1DOF the approach is sensible and is known to work, see [16].

Fig. 22 showed a good schematic illustration of the coupling points of an assembly for a representative wind turbine (source) and mounting system (receiver) system. From this figure, it is straightforward to see that the bearing of wind turbine and its mounting peripheral are connected by inserting the stub into the suitable hole of mounting pole.

During the actual mounting process, it was impossible or difficult to integrate even very small force sensors (with cables) into the coupling points between source and receiver unless modifying the source and/or receiver structure. Moreover, it is difficult to design the way how forces in the vertical direction which are perpendicular to the

wall plane could be measured at all, without the consideration of possible moments measurements about the x and y axes even. Modification of the source or receiver structure had been investigated and tested; however, this would reduce confidence level of the measurement of forces dramatically. Thus not a good option in this case.

Thus, for the instances which direct measurements are not available, the author had developed a novel alternative approach – indirect/inverse force determination which determines the force inversely from more easily obtained quantities: the vibration levels of structural response and relationship between excitation and response. This new method came out from the ideas of experiment and improved by theory of structural dynamics.

Above all, the force is easily to be written in the form of mass and acceleration which derived from Newton’s second law

$$F(\omega) = mA(\omega) \tag{6}$$

where A_0 is the amplitude of the acceleration expression of sinusoidal format regarding periodic forced vibration: $a(t) = A(\omega)\sin(\omega t + \phi)$. This is the simplest case of 1DOF and the test object had been considered as a rigid body without stiffness and damping. Furthermore, it is not a vibration case since (6) did not include the excitation frequency (ω). The acceleration levels could be measured and recorded by an accelerometer during the experiment.



Fig. 13 Front and side views of pier

Table 11 Comparison after second update

Mode number	Measured, Hz	Predicted, Hz	Error, %
1	3.678	6.5043	43.4528
2	9.589	13.095	26.7736
3	21.067	32.108	34.3871
4	27.86	39.609	29.6625
5	34.194	51.204	33.2201

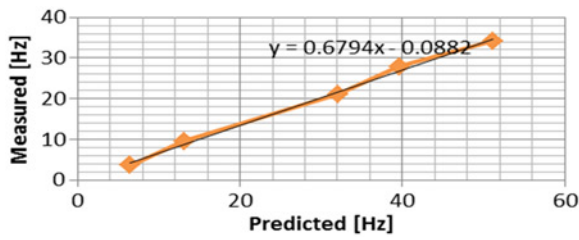


Fig. 14 Second update of correlation

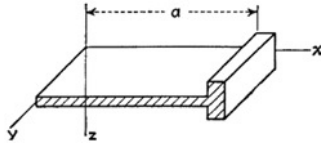


Fig. 15 Elastically supported

Table 12 Compared with predicted frequency of $E = 14$ GPa

Mode number	Measured frequency Hz	Predicted frequency, Hz for $E = 14$ GPa	Error, %
1	3.678	6.4637	43.0976
2	9.589	12.938	25.885
3	21.067	31.452	33.0186
4	27.86	39.242	29.0046
5	34.194	50.082	31.724

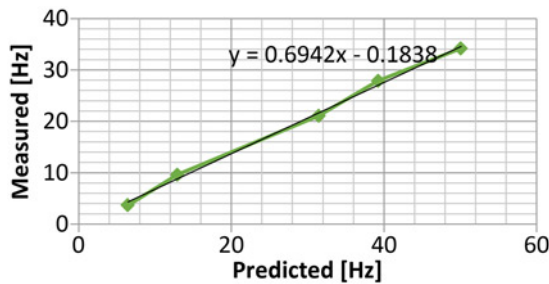


Fig. 16 Correlation for MATRIX27 with $E = 14$ GPa

However, the theory of structural dynamics would consider the impact of stiffness, damping and excitation frequency (ω). Thus, the initial method stated above had been developed by a steady-state solution of dynamic response in 1DOF

$$X(\omega) = H(\omega) \cdot F(\omega) \quad (7)$$

$H(\omega)$ is called the frequency response function (FRF) or transfer function. It is the ratio of displacement/force spectral and defined as a function of frequency (ω)

$$H(\omega) = \frac{R}{j\omega - p} + \frac{R^*}{j\omega - p^*}$$

$$R = -j \frac{1}{2m\omega_d} \quad R^* = j \frac{1}{2m\omega_d} \quad (8)$$

$$p = -\sigma + j\omega_d \quad p^* = -\sigma - j\omega_d$$

$$\omega_0^2 = \omega_d^2 + \sigma^2$$

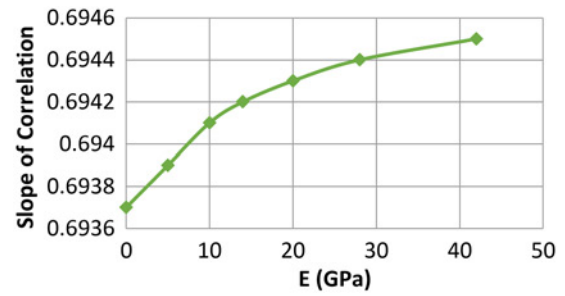


Fig. 17 Trend curve of E with a saturation point at $E = 14$ GPa

Table 13 Comparison of frequencies after FE fine tuning

Modal number	Measured frequency, Hz	Predicted frequency, Hz fine tuning	Error, %
1	3.678	6.4557	43.0271
2	9.589	12.927	25.8219
3	21.067	30.95	31.9321
4	27.86	38.458	27.5573
5	34.194	49.095	30.3514

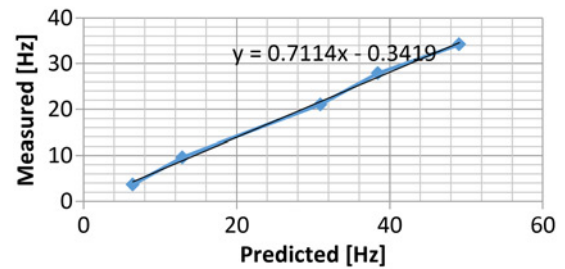


Fig. 18 Final correlation

In the equations, $H(\omega)$ is defined regarding two variables: p (pole location) and R (the residue), p^* and R^* denote their complex conjugates. The real part of p is the rate at which a vibration decays due to damping (σ). Its value is determined by half the -3 dB bandwidth of the FRF peak. The imaginary part is the damped natural frequency (ω_d) for a free damped vibration. Both p and R can be obtained from measurements of FRF. The FRF could be measured from an experimental modal analysis or structural testing indicated in the previous section. The deflection $X(\omega)$ is the amplitude of displacement. According to the physics, displacement is the double integral of acceleration.

If we want to obtain more accurate results, FEA is also employed to subdivide of a whole structure into simpler parts (FE) [17]. Previous models fall in a category of single DOF in a single movement direction. Complex structures usually have many points and several directions on each point – multiple DOFs totally. Thus

$$H_{ij}(\omega) = \frac{X_i(\omega)}{F_j(\omega)}$$

$$H_{ij}(\omega) = \sum_{r=1}^m H_{ijr}(\omega) \quad (9)$$

Index i is any response DOF, j is the arbitrary excitation DOF, r is any normal mode, m is number of modes used in this model. The whole calculation process could be achieved by MATLAB or

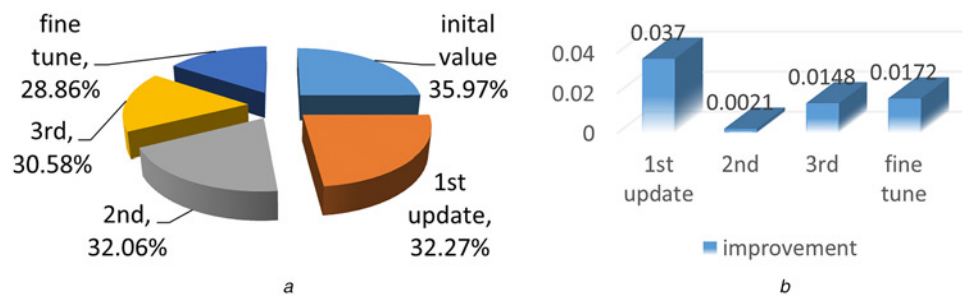


Fig. 19 Actual correlation is deviated from the target value of best fit for each updating procedure
a Percentage (%) of slope out of best fit
b Contribution of each updating step

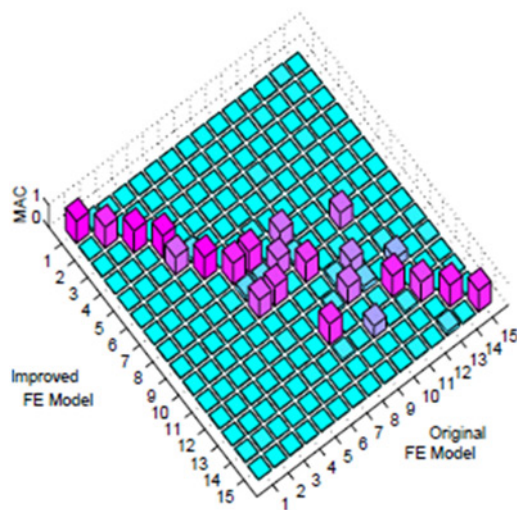


Fig. 20 MAC between initial prediction and measurement

other professional vibration software (such as LMS Lab test 12B) and the results were shown in the following figure (Fig. 23).

Once the force was determined, the harmonic analysis would be performed using ANSYS 12.0. The frequency of the load would be varied from 1 to 50 Hz (due to a maximal speed of 3000 rpm).

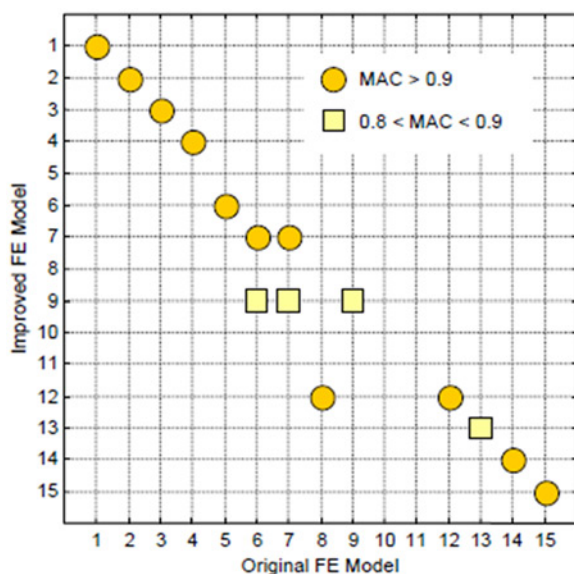


Fig. 21 Overhead view of MAC

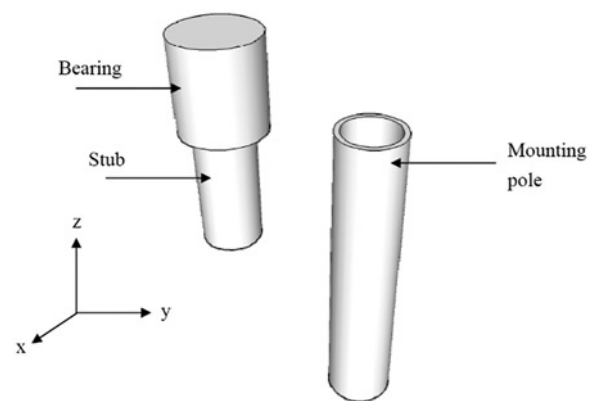


Fig. 22 Bearing, stub, mounting pole for coupling

Stepped BC (KBC) was chosen for the initial trial to ensure that the same amplitude (10 N) would be applied for each of the frequencies. The initial results from harmonic analysis were shown below (Fig. 24).

8 Measurement vibration level – a novel Lab simulation method

Though the predicted vibration level had been obtained, it was not robust and needs to be verified or validated by updating. Before doing the updating, the real/experimental vibration level should be measured by Lab testing. This requires a wind turbine mounted on the free stand wall of Lab (Fig. 1). However, the turbine could not work due to lack of strong wind inside Lab and we cannot employ a large fan to provide the wind power since it will blow off the whole lab! (a minimal wind speed of at least 5 m/s required). The author raised a new method to modify the internal configuration of the turbine and replaced the generator inside the turbine housing with a DC motor using electrical power supply.

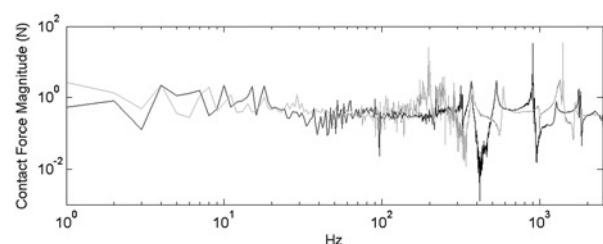


Fig. 23 Forces estimated from inverse method for two different contact points

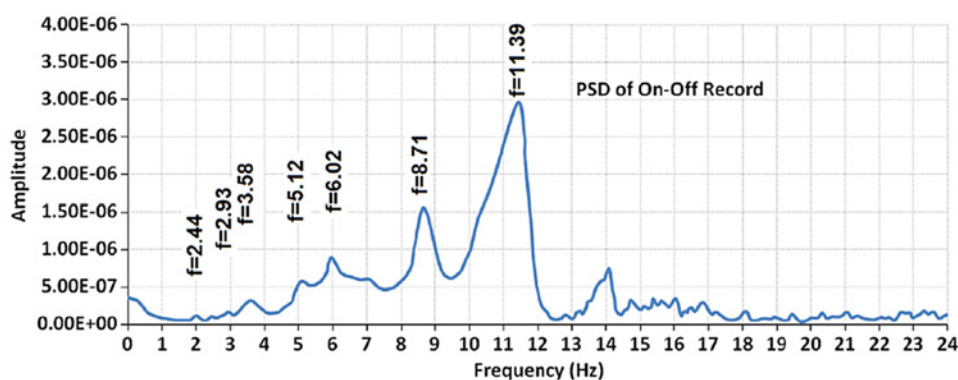


Fig. 24 Initial vibration level prediction within selected frequency range

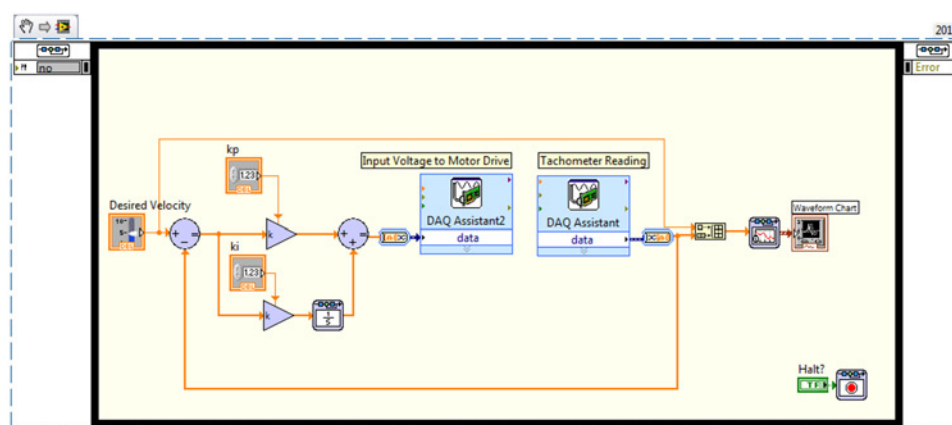


Fig. 25 *Diagram graph of PID controller*

The main difficulty of this lab simulation is the simulation of rotational speed in terms of RPM in Lab. In other words, we need to automatically control the motor's speed to the desired or expected value. The major part is a proportional–integral–derivative (PID) controller whose basic principle could be found everywhere in electrical engineering or control engineering without the needs to be repeated here. It will be converted to a computer program in LABVIEW of National Instruments (NI) which is shown in Fig. 25.

The NI PCI-6221 card has a built-in digital-to-analogue converter would output reference analogue in the range ± 10 V. The NI SC-2075 input/output (I/O) board has BNC connectors for

analogue I/Os. The Copley Control 300 series servo amplifier operates from 16 to 80 V input provided by DC power supplies. The DYNATEC 110 V transformer and Copley Control series 600 power supplies have been designed to compliment Copley Control servo amplifiers and to provide the user with a 65 V (8 A) DC drive applications. To mount the amplifier and make it working you will need a reference voltage which is from the digital control system (PID). The amplifier is usually used as a voltage-to-current converter as a basic function. Here, ± 10 V reference signals will drive the amplifier's peak rated current in a called 'flat-gain' mode. The principle of this mode is to force a reference voltage inputs to a current outputs in amplifier. Flat-gain means the maximum bandwidth provided by it remains constant over the 3 kHz range. The peak power output for 306 amplifier is ± 75 V at ± 25 A; the maximum continuous current is 10 A. The amplifier connections were shown in Fig. 26. Connect DC power supply to amplifier, connect motor between OUT+ and OUT, connect outputs spring terminals of SC-2075 I/O board to + and - ref. inputs, make sure the ENABLE, POS ENABLE and NEG ENABLE ports connected together with logic ground of servo amplifier 306.

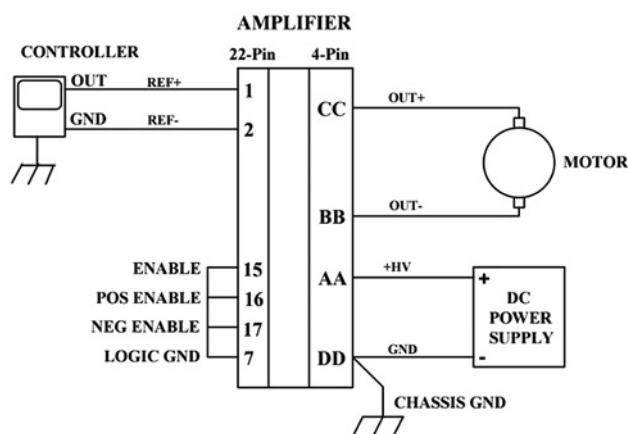


Fig. 26 *Amplifier connections*

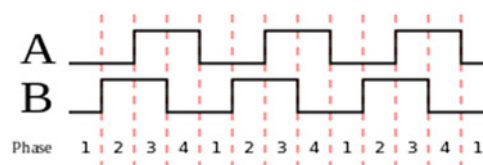


Fig. 27 *Two square signals in quadrature out of 90°*

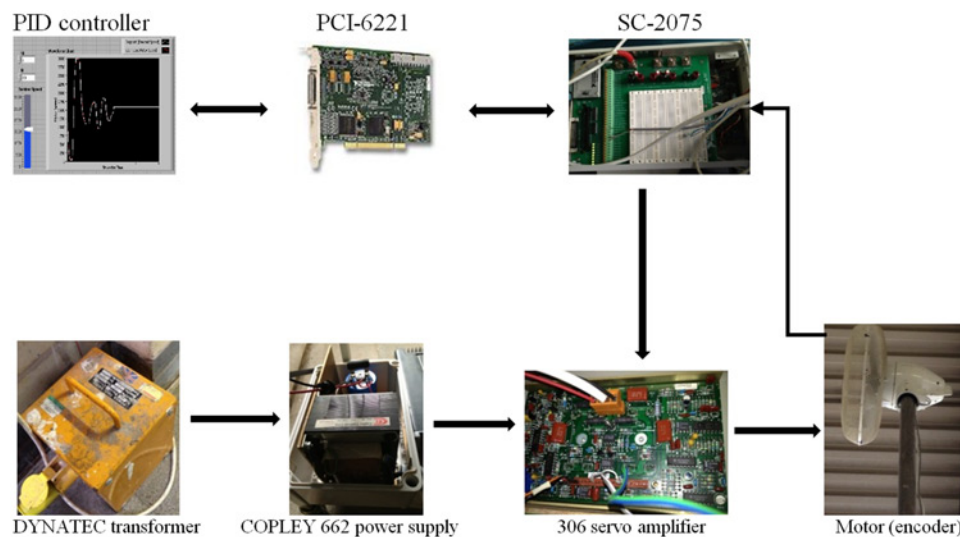


Fig. 28 600 W DC motor speed control using LABVIEW PID

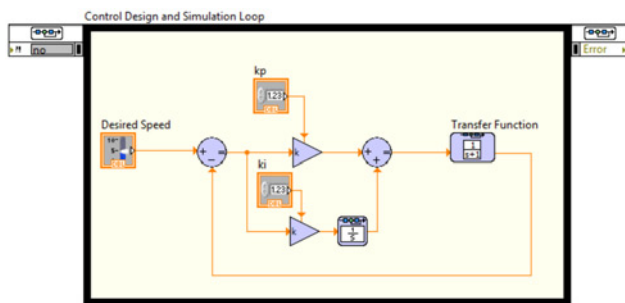


Fig. 29 PI controller in LABVIEW

The PID control systems would get speed feedback from an encoder of a servo motor. Transducer (e.g. tachometer or encoder) perceived the position or velocity in the format of a feedback signal to controller. A rotary encoder converts rotary position or physical parameter of motor movement to an analogue or digital quadrature electronic signal. An incremental rotary encoder provides pulse outputs and employs two signals called A and B, which are quadrature since out of phase by 90° (Fig. 27). These signals are decoded in PCI-6221 card to a count up or down pulse.

The SC-2075 contains spring terminal access to the digital I/O channels of the PCI-6221 DAQ device with these timing and control I/O signals. M series PCI-6221 devices have two general purpose 32 bit counter/timers and can be used for counting edges.

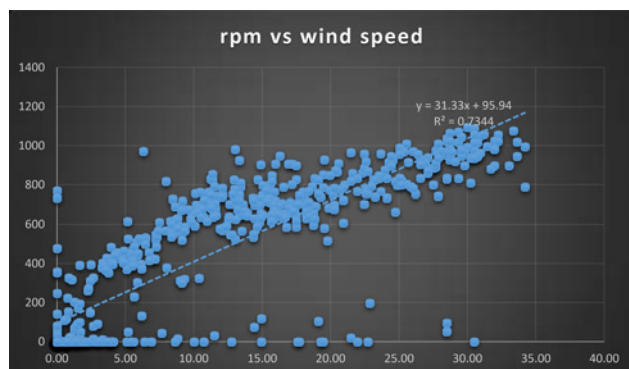


Fig. 30 A600-rotor speed against wind speed (10 s average data)

The rotational speed could be easily calculated from the relationship between the number of edge counting, revolution and pulse. The whole control process had been displayed as a flowchart (Fig. 28) for explanation.

In this paper, a PI controller for 600 W DC motor was designed using LABVIEW control design and simulation module (Fig. 25).

The next step is to simulate the response of the DC motor when modifying the set-point or desired speed input (Fig. 29). The desired speed (available test data) were generated and collected from our industrial partner – Ampair Wind Turbine Ltd. More than 10,000 sample data were obtained during a long-term observation (Fig. 30), the rpm is pulses averaged over 10 s period. Some representative real rotational speed data were shown in Table 14. A 10 min time history (scenario) of RPM was plotted from the test data for PID control (Fig. 31).

Once the speed profile was input to the computer, the wind turbine would be working under desired wind conditions due to a real lab simulation. Moreover, the experimental vibration levels could be measured afterwards (Fig. 32).

9 Vibration response updating (resonant frequency)

Once both the theoretical and experimental harmonic response (Figs. 24 and 32) had been obtained, the most important modal parameter (resonant frequency) in forced vibration behaviour should be validated during an updating process. Above all, the initial comparison between two different sets of data had been indicated in Fig. 33.

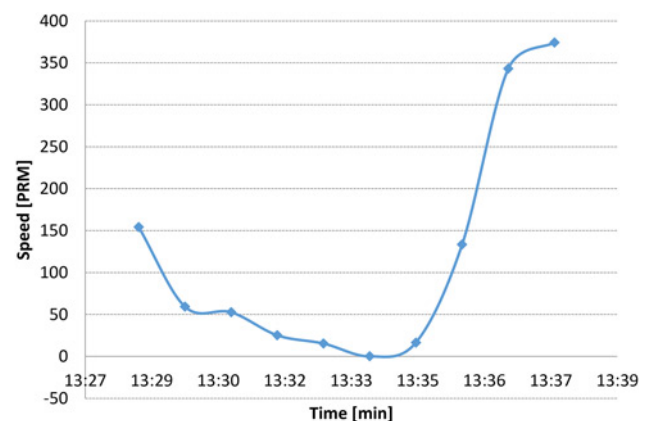
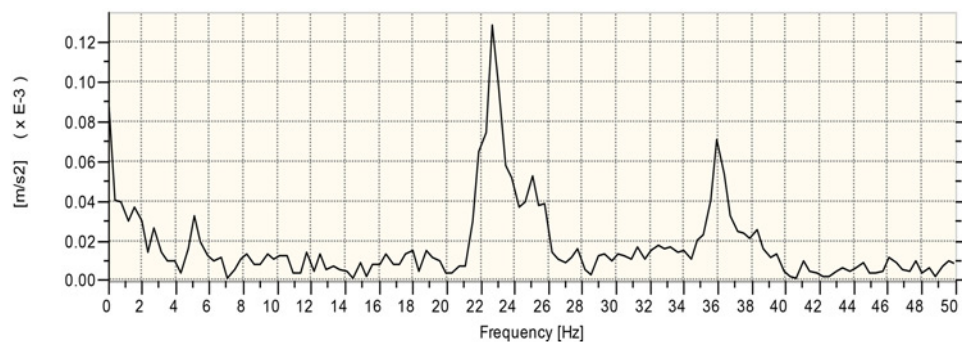


Fig. 31 Plot of RPM time history against time

Table 14 Representative RPM recording during 20 min

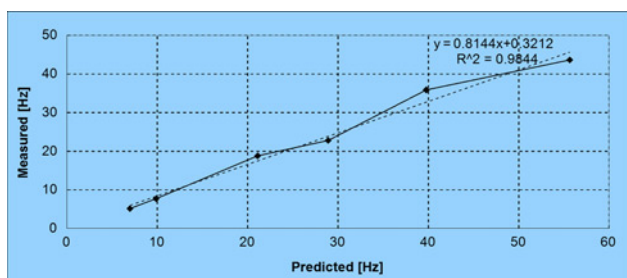
Time, s	0	10	20	30	40	50	60	70	80
speed, rpm	1088.9	1077.1	1094.8	1056.3	1071.4	1016.9	995	1025.6	1056.3
time, s	90	100	110	120	130	140	160	170	180
speed, rpm	986.8	1018.6	946.3	981.9	1023.8	1045.2	1038	1020.4	940.4
time, s	190	200	210	220	230	240	250	260	270
speed, rpm	1065.7	789.4	1022.1	967.7	978.7	1050.7	886.2	944.8	1058.2
time, s	280	290	300	310	320	330	340	350	360
speed, rpm	916	950.8	1015.2	963	928.7	956.9	1015.2	947.8	941.9
time, s	370	380	390	400	410	420	430	440	450
speed, rpm	975.6	1010.1	923	952.3	993.3	991.7	925.9	913.2	890.2
time, s	460	470	480	490	500	510	520	530	540
speed, rpm	898.2	931.6	996.6	937.5	810.8	920.2	931.6	990	833.3
time, s	550	560	570	580	590	600	610	620	630
speed, rpm	969.3	860.8	928.7	868.3	834.4	910.4	755.6	859.5	847.4
time, s	640	650	660	670	680	690	700	710	720
speed, rpm	776.1	872	907.7	859.5	937.5	903.6	773.1	801	884.9
time, s	730	740	750	760	770	780	790	800	810
speed, rpm	744.4	805.3	918.8	865.8	791.5	750	833.3	910.4	899.5
time, s	820	830	840	850	860	870	880	890	900
speed, rpm	824.1	790.5	907.7	704.2	786.3	741.6	832.1	749	767.2
time, s	910	920	930	940	950	960	970	980	990
speed, rpm	750	788.4	791.5	869.5	818.5	758.5	847.4	833.3	907.7

**Fig. 32** Measurement vibration level in frequency domain

It is obvious that the second updating process makes a further improvement toward the perfect correlation. This is an improvement to target of only 0.0341 but it should be included in the updating process for reference. The final correlation value is only 0.014 (1.4%) away from perfect unity.

9.1 Summary

The methodology to predict these impacts (FEA) should be now sufficiently robust that decisions relating to the amenity (and not merely) of neighbouring properties can be predicted. This is achieved by

**Fig. 33** Initial correlation between predicted and measured resonant frequencies

testing a hypothesis through laboratory/field tests on a statistically valid sample size (statistical analysis) and through a series of rigorous FEMs (numerical analysis) by validating and verifying the above hypothesis using numerical and analytical (mathematical) models.

10 Concluding comments

- To achieve motor speed control, the real-time wind profile data should be read from a file (text or XL) one by one with a few milliseconds time delay. An index array function would be used to get the column required and be wired to a for loop with a 'Wait Until Next ms Multiple' inside the loop.
- The number of DOFs has to be chosen to represent the total dynamics of the structure. It is the geometrical complexity of the mode shapes, rather than to the number of modes expected, which determines the number of DOFs required.
- There is relatively good agreement between mode shapes from the experimental and the FE modal analysis. Mode 1 is the fundamental bending mode of vibration. Mode 2 is of some interest as an almost predominantly torsional mode also showing small amount of bending and Mode 3 similar to Mode 2. It would be very difficult to interpret it without the help of FEA. Note that plane symmetry has been applied to all FE-models, and therefore only half the models are shown. It should be stressed again that without the help of the FEA it would be difficult to interpret any complex modes based

on the experimental results alone. Modes 2 and 3 represent twisting tendencies of the rectangular plane-shape thin plate unit (depicted successfully in the FEA), whereas modes 4 and 5 maybe regarded as the second and third 'bending-like' modes of vibration. Mode 5 also inhibits a small amount of torsion.

11 Acknowledgments

The financial support of the Engineering Faculty of Sheffield University and Ampair Wind Turbine Ltd. for all materials for testing (turbines, their peripherals, installation, know-how etc.) provided as in-kind support is gratefully acknowledged. The collaborating company invested a nominal amount of cash in the project and team-up in an EPSRC studentship application, is much appreciated. Also the author expresses his gratitude to Mr. Ian Breakwell, senior technician at the Structural Engineering Lab for his kind support to set up the test rig. Special mention should also be made of Mr. Steve Hutton, the electrical technician in the department for help and suggestions of the motor speed control progress. At last, the author would be grateful to Mr. David Sharman, the head of our industrial partner, for his permission to do a field test in-situ.

12 References

- [1] Wilson E.L., Habibullah A.: 'SAP2000 – structural analysis users manual' (Computers and Structures, Inc., 1998)
- [2] Timoshenko S.P., Woinowsky-Krieger S.: 'Theory of plates and shells' (McGraw-Hill, 1959)
- [3] Nichols J.M., Totoev Y.Z.: 'Experimental determination of the dynamic modulus of elasticity of masonry units'. 15th ACMSM, 1997
- [4] Pande G.N., Liang J.X., Middleton J.: 'Equivalent elastic moduli for brick masonry', *Comput. Geotech.*, 1989, **8**, (3), pp. 243–265
- [5] Sassoni E., Mazzotti C., Pagliai G.: 'Comparison between experimental methods for evaluating the compressive strength of existing masonry buildings', *Constr. Build. Mater.*, 2014, **68**, pp. 206–219
- [6] Erdogmus E., Boothby T.: 'Strength of spandrel walls in masonry arch bridges', *Transp. Res. Res. J. Transp. Res. Board*, 2004, **1892**, pp. 47–55
- [7] EN 1996-1-1 (English): 'Eurocode 6: design of masonry structures – part 1-1: general rules for reinforced and unreinforced masonry structures' [Authority: The European Union Per Regulation 305/2011, Directive 98/34/EC, Directive 2004/18/EC], 2005
- [8] EN 1996-3 (English): 'Eurocode 6: design of masonry structures – part 3: simplified calculation methods for unreinforced masonry structures' [Authority: The European Union Per Regulation 305/2011, Directive 98/34/EC, Directive 2004/18/EC], 2006
- [9] EN 998-2: 'Specification for mortar for masonry – part 2: masonry mortar'
- [10] BS EN 771-1: 'Specification for masonry units. Clay masonry units', 2011
- [11] BS NA EN 1996-3 (English): 'UK national annex to Eurocode 6. Design of masonry structures. Simplified calculation methods for unreinforced masonry structures', 2006
- [12] Kwak H.-G., Filippou F.C.: 'Finite element analysis of reinforced concrete structures under monotonic loads'. Structural engineering mechanics and materials, PhD thesis, Department of Civil Engineering University of California, Berkeley, California, Report No. UCB/SEMM-90/14, 1990
- [13] Song H.-W., Shim S.-H., Byun K.-J., *ET AL.*: 'Failure analysis of reinforced concrete shell structures using layered shell element with pressure node', *J. Struct. Eng.*, 2002, **128**, (5), pp. 655–664
- [14] Sherif A.G., Dilger W.H.: 'Analysis and deflections of reinforced concrete flat slabs', *Can. J. Civil Eng.*, 2006, **25**, (3), pp. 451–466
- [15] Karadelis J.N.: 'Concrete grandstands. Part I. Experimental investigation', *Proc. Inst. Civil Eng. Eng. Comput. Mech. J.*, 2009a, **161**, (EM1), pp. 3–9, doi: 10.1680/eacm.162.1.3
- [16] Lai H.Y.: 'Experimental comparison of test methods for structure-borne sound power measurement'. SAE 2007 Noise and Vibration Conf. and Exhibition, 2007
- [17] Reddy J.N.: 'An introduction to the finite element method' (McGraw-Hill, New York, NY, USA, 2006, 3rd edn.), ISBN 9780071267618